

## CFD Simulation of the NUPEC BWR Full-size Fine-mesh Bundle Test for a Void Distribution Benchmark

Wang-Kee In<sup>a\*</sup>, Dae-Hyun Hwang<sup>a</sup>, Tae-Hyun Chun<sup>a</sup>

<sup>a</sup>Korea Atomic Energy Research Institute

\*Corresponding author: wkin@kaeri.re.kr

### 1. Introduction

A computational fluid dynamics (CFD) analysis is performed to predict a steady-state void distribution in a BWR fuel bundle. OECD/NRC organized the BWR full-size fine-mesh bundle test (BFBT) benchmark [1] based on data made available from the Nuclear Power Engineering Corporation (NUPEC). The NUPEC provided measured void distribution data in a fuel bundle for the BFBT benchmark. This CFD study simulated the four experimental conditions for thermodynamic quality of 2%, 5%, 12% and 25% at the outlet of test bundle, i.e., high burn-up 8x8 fuel bundle with single water rod. The CFD predictions of void distributions are compared with the measurements in microscopic grade (0.3 mm x 0.3 mm) and subchannel grade.

### 2. Numerical Methods

#### 2.1 CFD Model and Boundary Condition

The NUPEC performed measurements of a void fraction distribution in a BWR fuel assembly. An electrically heated rod bundle has been used to simulate a full scale BWR fuel assembly. The test fuel assembly is 8x8 rod bundle with 60 fuel rods plus single water rod and 7 ferrule-type spacers. The outer diameter and pitch of 60 heated rods are 12.3mm and 16.2mm, respectively. The heated length of test rod bundle is 3708mm with an axially uniform heating. The radial power profile of test assembly is given in Table 1.

Using symmetry of geometry and radial power shape, half of the test bundle in fully heated length was simulated in this study. The spacers of the test bundle are not included in this CFD simulation because its effect on void distribution is not judged to be large. A hexahedral mesh is used and the total number of nodes is 4.72 million with axial nodes of 151 in streamwise direction. The lateral space between the nodes is 0.2mm near the rod surface and 1.2mm in the center of the subchannels.

Table 1 Radial power shape of test assembly

1.15	1.30	1.15	1.30	1.30	1.15	1.30	1.15
1.30	0.45	0.89	0.89	0.89	0.45	1.15	1.30
1.15	0.89	0.89	0.89	0.89	0.89	1.15	1.15
1.30	0.89	0.89			0.89	0.89	1.15
1.30	0.89	0.89			0.89	0.89	1.15
1.15	0.45	0.89	0.89	0.89	0.89	0.45	1.15
1.30	1.15	0.45	0.89	0.89	0.45	1.15	1.30
1.15	1.30	1.15	1.15	1.15	1.15	1.30	1.15

A uniform flow and constant pressure are assumed at the inlet and outlet boundaries, respectively. A constant heat flux is applied on the fuel rods and adiabatic conditions on the water rod and the shroud. Working fluid is water at 7.2 MPa. The flow rate is 55 ton/h and inlet subcooling is 51-53 kJ/kg.

#### 2.2 Numerical Procedure

A CFD code, ANSYS CFX-10.0 [2], was used in this study. Inhomogeneous multiphase flows are assumed to simulate the liquid and gas(vapor) phases which are considered to be continuous and dispersed fluids, respectively. The vapor phase is assumed to be dispersed with mean diameter of 2.0mm. The two fluids interact via interphase transfer terms based on a particle model, i.e., interphase momentum transfer and heat transfer. The interfacial forces acting between two phases included in this study are the interphase drag, lift force, wall lubrication force and turbulent dispersion force.

The interphase heat transfer uses the two resistance model to consider separate heat transfer processes on either side of the phase interface. A constant Nusselt number (1000) is used for liquid interphase heat transfer. A zero resistance condition for the interphase heat transfer is applied at the vapor side to force the interfacial temperature to be the same as the vapor-phase temperature, i.e., the saturation temperature.

Iterative calculations were performed to obtain a converged solution with a false time step of 0.001 sec and a high resolution differencing scheme. The numerical iteration was continued until both the root-mean-square(RMS) residuals of governing equations and the variation of flow properties monitored at specified locations are insignificant. The RSM residuals of governing equations were decreased to below 1.0e-06 for the phasic momentum and volume fraction conservation, and 1.0e-04 for the energy and turbulence conservation. In addition, the velocity and volume fraction of liquid and vapor monitored at the outlet boundary were converged to their steady-state values.

### 3. Results and Discussion

The four test cases (TS4101-53, 55, 58, 61) for the BFBT benchmark were simulated in this CFD study to predict the void distribution. Table 2 lists the cross-sectional averaged void fraction at the exit of heated section. The CFD predictions agree well with the measurements for the conditions of a low exit quality but show a large difference up to 12% for the high quality cases.

Table 2 Cross-sectional averaged exit void fraction

Test case	Exit quality	CFD	Measured
TS4101-53	2%	24.7	25.0
TS4101-55	5%	43.4	43.8
TS4101-58	12%	59.2	64.5
TS4101-61	25%	70.9	80.7

The void distribution at the outlet of the test bundle is compared in Fig. 1 for the test case TS4101-55. The measured one shows the raw image data obtained from the X-ray CT scanner which has a spatial resolution as small as 0.3mmx0.3mm. The CFD simulation shows a reasonable radial void distribution trend predicting less vapor in the central region of the bundle and more vapor in the periphery. Unlike measured data, the CFD prediction shows higher concentration of vapor near the rod surfaces instead in the center of the subchannels.

Table 3 compares the subchannel averaged void fraction predicted by the CFD(CFX) code and MATRA(subchannel analysis code [3]) with respect to the measured one. Subchannel 1 represents a guide thimble subchannel surrounding the water rod. Subchannels 2 and 3 are the interior matrix subchannels next to the subchannel 1. Subchannels 4 and 5 are the side and corner channels, respectively. The CFD calculation shows a large over-prediction in the corner channel and under-prediction in the interior subchannel 2. The MATRA code predicted a somewhat higher void fraction in the water rod channel but a lower void in the side subchannel.

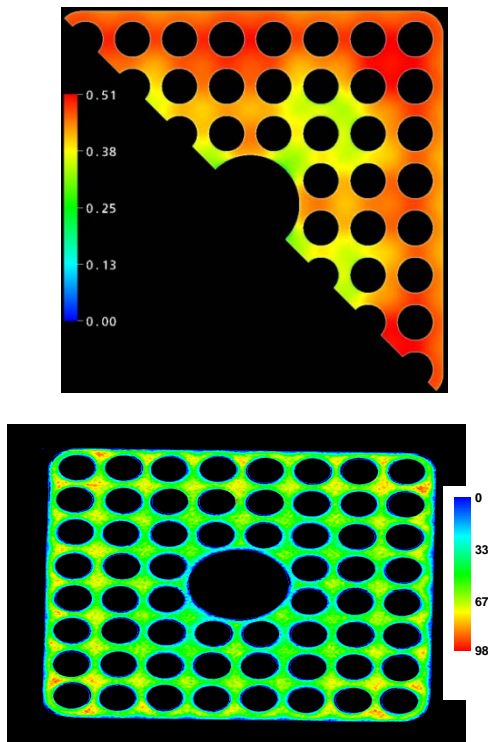


Fig. 1 Void distributions at the exit of BFBT rod bundle(TS4101-55); (above) predicted(CFX), (below) measured

Table 3 Subchannel averaged exit void fraction(TS4101-55)

Subchannel	1	2	3	4	5
Measured	31.7	43.6	49.4	52.2	38.9
MATRA	36.9	42.2	48.4	44.6	37.7
CFD(CFX)	34.7	35.5	50.6	47.2	47.0
Error(CFX)	9.4	-18.6	2.4	-9.6	20.8

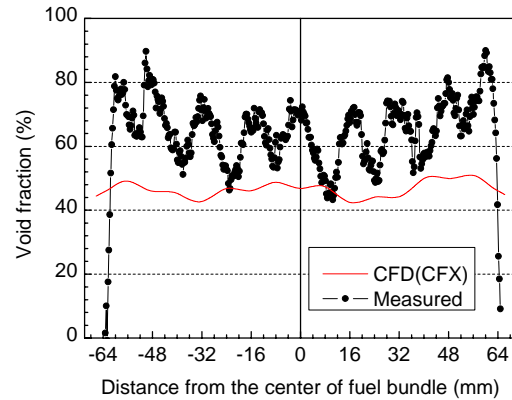


Fig. 2 Lateral void distribution along the centerline between fuel rods(TS4101-55)

Figure 2 shows the comparison of the void distribution along the centerline between the first and second rows of fuel array. The CFD simulation predicts a much lower void than the measured one in the center of the subchannels. The variation of the void fraction between the subchannel center and the rod gap is about 5% for the CFD and 20% for the measured. This discrepancy is mainly due to not properly predicting the void peaking measured in the center of the subchannels.

#### 4. Conclusions

An international benchmark for a void distribution in a BWR fuel bundle was simulated by using the CFD code. The CFD analysis predicted the cross-sectional averaged void fraction which agreed reasonably well with the measured one. The CFD simulation also reproduced the overall radial void distribution trend which is less vapor in the central part of the bundle and more vapor in the periphery. However, the CFD simulation was not able to predict a very high concentration in the center of the subchannels. It is therefore necessary to develop a multiphase flow model which can properly predict the void drift inside a subchannel as well as between subchannels in a rod-bundle geometry.

#### REFERENCES

- [1] US NRC, OECD NEA, NUPEC BWR Full-Size Fine-Mesh Bundle Test (BFBT) Benchmark, Volume 1: Specifications, NEA/NSC/DOC(2005)5, November 2005.
- [2] ANSYS Inc., ANSYS CFX, Release 10.0, 2005.
- [3] Y. J. Yoo, D. H. Hwang and D. S. Sohn, "Development of a Subchannel Analysis Code MATRA Applicable to PWRs and ALWRs," J. Korean Nuclear Society, Vol.31, p.314, 1999.